Corona Composition Can Affect the Mechanisms Cells Use to Internalize Nanoparticles

Francia, Valentina; Yang, Keni; Deville, Sarah; Reker-Smit, Catharina; Nelissen, Inge; Salvati, Anna

Published in:
Acs Nano

DOI:
10.1021/acsnano.9b03824

Publication date:
2019

ACS NANO

Cite This: ACS Nano 2019, 13, 11107−11121

www.acsnano.org

ARTICLE

Corona Composition Can Affect the Mechanisms Cells Use to Internalize Nanoparticles

Valentina Francia,[†] Keni Yang,[†] Sarah Deville,[‡,§] Catharina Reker-Smit,[†] Inge Nelissen,[‡] and Anna Salvati*[,†]

[†]Department of Pharmacokinetics, Toxicology and Targeting, Groningen Research Institute of Pharmacy, University of Groningen, Antonius Deusinglaan 1, 9713AV Groningen, The Netherlands

[‡]Health Department, Flemish Institute for Technological Research (VITO), Boeretang 200, 2400 Mol, Belgium

[§]Biomedical Research Institute, Hasselt University, Agoralaan building D, 3590 Diepenbeek, Belgium

Supporting Information

ABSTRACT: **Nanosized objects, such as nanoparticles and other drug carriers used in nanomedicine, once in contact with biological environments are modified by adsorption of biomolecules on their surface. The presence of this corona strongly affects the following interactions at cell and organism levels. It has been shown that corona proteins can be recognized by cell receptors. However, it is not known whether the composition of this acquired layer can also affect the mechanisms nanoparticles use to enter cells. This is of particular importance when considering that the same nanoparticles can form different coronas for instance *in vitro* when exposed to cells in different serum amounts or *in vivo* depending on the exposure or administration route. Thus, in this work, different coronas were formed on 50 nm silica by exposing them to different serum concentrations. The uptake efficiency in HeLa cells was compared, and the uptake mechanisms were characterized using transport inhibitors and RNA interference. The results showed that the nanoparticles were internalized by cells *via* different mechanisms when different coronas were formed, and only for one corona condition was uptake mediated by the LDL receptor. This suggested that coronas of different composition can be recognized differently by cell receptors, and this in turn leads to internalization *via* different mechanisms. Similar studies were performed using other cells, including A549 cells and primary HUVEC, and different nanoparticles, namely 100 nm liposomes and 200 nm silica. Overall, the results confirmed that the corona composition can affect the mechanisms of nanoparticle uptake by cells.**

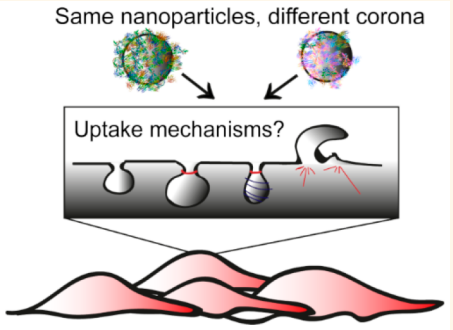

KEYWORDS: *biomolecule corona, nanoparticle, uptake mechanisms, transport inhibitors, silica*

Nanosized materials are widely investigated for their potential use as drug delivery systems thanks to their ability to distribute in the body and enter cells and the possibility to engineer them for multiple purposes.[1−3] Several nanomedicines are already on the market; however it is recognized that a better understanding of the mechanisms by which these objects are processed at organism and cell levels could contribute to further advance their clinical success.[4−6]

In recent years, particular interest has been drawn on the impact of the biological environment in which nanomaterials are applied on their interactions at the organism and cellular level. Once in contact with a biological environment, nanosized objects immediately interact with the surrounding biomolecules, which can adsorb on the nanoparticle surface, leading to the formation of a biomolecular corona.[7,8] Some of the biomolecules in this layer associate with the nanoparticle surface almost irreversibly, affecting *de facto* the subsequent behavior. For instance, it has been shown that the formation of the corona can affect nanomaterial stability and biodistribution, macrophage sequestration, immune system activation, cellular recognition, and nanomaterial final fate.[9−11] In some cases, the formation of a biomolecular corona can also affect the specificity of targeted drugs, by masking targeting ligands attached to the nanocarrier.[12,13] Polymers such as poly(ethylene glycol) (PEG) are usually grafted on the nanoparticle surface to partially reduce protein binding and subsequent macrophage sequestration.[14−16] However, recent work suggested that the so-called stealth effect is actually conferred by specific corona proteins adsorbed on PEGylated

Received: May 16, 2019
Accepted: September 17, 2019
Published: September 17, 2019

DOI: 10.1021/acsnano.9b03824
ACS Nano 2019, 13, 11107−11121

surfaces.[17] At the same time, researchers are also trying to exploit the biomolecular corona as a targeting strategy to direct nanoparticles toward specific cellular routes.[18−20]

So far, corona formation and its composition have been widely investigated.[21−24] It is known that different nanoparticle properties such as size, charge, and shape can influence corona composition, and this can lead to different cellular responses to nanomaterials.[8,25,26] The corona composition also varies depending on the nature of the biological fluids in which nanoparticles are dispersed, such as fetal bovine serum, human serum, or plasma,[27] and even in the same fluid, when the ratio between nanoparticle and fluid concentration is changed.[28] It has also been shown that the composition of this layer evolves over time or for instance during nanoparticle exposure to cells, because of adsorption of biomolecules secreted by cells in the medium.[21,22,29,30]

Importantly, several studies have highlighted that the corona composition affects nanoparticle−cell association[31] and that corona proteins can engage with specific cell receptors.[10,20,32,33] For instance, it has been shown that the uptake of silica nanoparticles is mediated by the recognition of corona proteins by the low density lipoprotein (LDL) receptor.[10] However, it is not known yet whether the corona composition and the initial recognition of corona proteins by specific cell receptors also affect the following mechanism cells use to internalize the nanoparticles.

To this aim, in this work we characterized and compared the mechanisms of uptake of nanoparticles dispersed in media containing two very different serum concentrations, a high serum content close to protein concentration in blood (roughly 60 mg/mL) and a 5 times lower one. Silica nanoparticles (SiO_2 nanoparticles) of 50 nm diameter were used as a representative model system to form different coronas in the two conditions. It is known that varying serum amount can lead to formation of different coronas.[28] Then, the effect of serum content on the uptake efficiency in HeLa cells was investigated, and common pharmacological inhibitors of endocytosis were used in order to determine potential differences in the mechanisms of uptake in the two conditions. Next, RNA interference was used to silence the expression of the LDL receptor, here selected as a first illustrative example, given the previous reports on its involvement in the uptake of similar silica nanoparticles.[10] This allowed us to test its involvement in the initial recognition of the corona proteins by cells. Finally, similar experiments were performed on different cells, *i.e.* A549 cells and primary human umbilical vein endothelial cells (HUVEC), and with different nanoparticles, including 200 nm silica and 100 nm 1,2-dioleoyl-*sn*-glycero-3-phospho-(1′-*rac*-glycerol) (DOPG)−cholesterol liposomes, in order to translate the results to other systems. In this way, we have been able to connect the effect of corona composition on the initial recognition by specific cell receptors (here the LDL receptor) with the following mechanisms cells use to internalize nanoparticles.

RESULTS AND DISCUSSION

Characterization of the Corona−Nanoparticle Complexes. Silica of 50 nm were selected as a well-characterized model nanoparticle. Extensive information on their corona properties and interactions with cells is already available.[21,28,34,35] Furthermore, thanks to their density, simple centrifugation can be used to separate corona-coated nanoparticles from the unbound serum biomolecules, making isolation of corona−nanoparticle complexes relatively easy (see Methods and Supplementary Table S1 for details).

In order to form different coronas and study their effect on cellular uptake mechanisms, the nanoparticles were dispersed in two very different serum amounts, a lower and a roughly 5 times higher serum concentration (12 and 62 mg/mL proteins, respectively). Instead of standard fetal bovine serum, pooled human serum was used as a more relevant serum source when testing uptake mechanisms on human cells. Similarly, as a first step, serum was selected instead of plasma to avoid additional complications related to the choice of the anticoagulant used to prepare it.[36]

Exposure of nanoparticles to different amounts of proteins may also affect particle stability, and this, in turn, could affect the resulting interactions with cells.[37−39] Thus, the nanoparticle dispersions in (MEM) cell media supplemented with the different amounts of serum and the corresponding corona−nanoparticle complexes (low-serum and high-serum corona−nanoparticle complexes, LC and HC, respectively) were characterized by dynamic light scattering (DLS) and differential centrifugal sedimentation (DCS) (see Figure 1A, Supplementary Figure S1, and Supplementary Tables S2 and S3 for details). In some cases, DLS showed small peaks at larger sizes, suggesting the presence of micrometer-sized agglomerates. However, the DCS results on the isolated corona complexes allowed us to exclude the presence of large agglomerates and confirmed that fairly homogeneous dispersions of isolated corona complexes were obtained, including small agglomerates (such as dimers, trimers, and similar) in the case of the complexes formed in lower serum (Figure 1A and Supplementary Table S2).

Next, SDS-PAGE was used to confirm, that—as previously reported for similar nanoparticles[28]—the dispersion in different serum concentrations led to adsorption of different amounts and types of proteins on the surface of the nanoparticles (Figure 1B, with arrows indicating for illustration some examples of differences in the bands detected).

Mass spectrometry was used to characterize the corona composition (Figure 1C, Table 1, and full list in the Supporting Information). About 300 different proteins were identified in both samples, with the 15 most abundant ones contributing alone to roughly 36% (HC) and 50% (LC) of the total proteins recovered. As already observed for similar studies, although most of the proteins were present in both coronas, the relative abundance of some of them was very different between the two samples. For instance, while apolipoprotein B-100 content was comparable in the two cases, the histidine-rich glycoprotein was particularly enriched in the corona formed at high serum amount, and *vice versa* apolipoprotein A-I content was much higher in the corona formed in low serum.

Nanoparticle Uptake Efficiency *in Situ* and after Corona Isolation. As a next step, the cellular uptake efficiency of the silica nanoparticles in the different serum conditions was tested. To this aim, HeLa cells were used as a standard cell model commonly applied for similar uptake studies, in both the endocytosis and nanomedicine fields.[40−42] Cells were exposed to the nanoparticles in the presence of low and high serum content *in situ* or after isolation of the corona−nanoparticle complexes and removal of the free proteins in solution (Figure 2). As already reported in the literature, the uptake efficiency in the presence of a high amount of serum was much lower than for nanoparticles incubated with a low

DOI: 10.1021/acsnano.9b03824
ACS Nano 2019, 13, 11107−11121

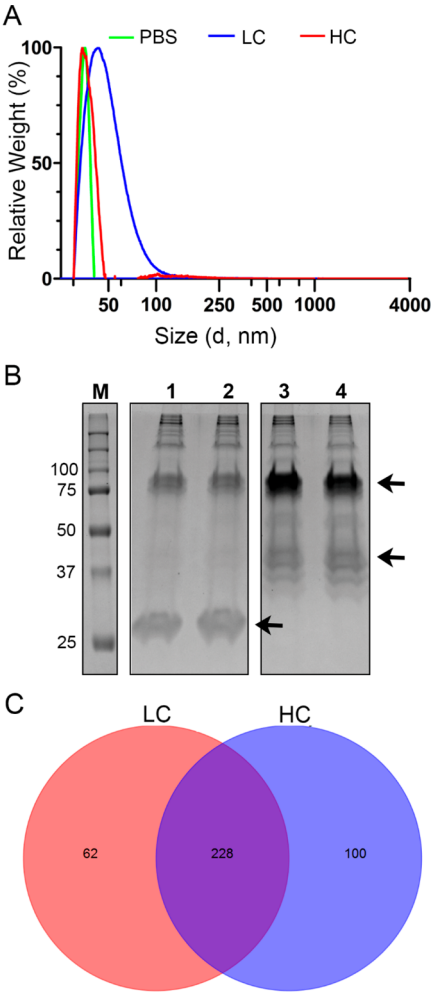

Figure 1. Characterization of the corona formed on 50 nm silica nanoparticles in low and high serum content (LC and HC, respectively). (A) Differential centrifugal sedimentation (DCS) of 50 nm silica nanoparticles in PBS and the corona−nanoparticle complexes formed in low or high amount of serum (LC and HC, respectively), performed as described in the Methods (see also Supplementary Table S2). (B) SDS-PAGE gel image of the proteins recovered from corona−nanoparticle complexes formed in low (lane 1 and 2) or high (lane 3 and 4) human serum and isolated after 30 min (lane 2 and 4) or 1 h (lane 1 and 3) centrifugation. The corona formed on 300 μg/mL silica nanoparticles dispersed in 12 and 62 mg/mL human serum, respectively, was prepared and isolated as described in the Methods. The gel shows that different bands were present in the two conditions (arrows indicate some examples). M: molecular weight ladder. (C) Venn diagram of the total amount of proteins identified by mass spectrometry in the corona−nanoparticle complexes formed in the two conditions.

amount of serum.[10,12] This can be explained—at least in part—by the presence of a high amount of free serum biomolecules in solution. Since the corona biomolecules can mediate the uptake of nanoparticles through recognition by specific cellular receptors,[8,10,12] it is likely that the free serum proteins in solution might also compete for the same receptors and, in this way, reduce the uptake levels of the corona−nanoparticle complexes. Indeed, the uptake was higher when the corona−nanoparticle complexes were isolated and the free proteins in solution were removed. Given the very different uptake efficiency, in order to focus solely on the effect of corona composition on the mechanisms of uptake and exclude additional effects due to the interference of the free serum molecules in the process, the following studies were performed using isolated corona−nanoparticle complexes. However, it is interesting to note that even after removal of the excess free

Table 1. List of the Most Abundant Proteins Identified in the Corona Formed on 50 nm Silica Nanoparticles in Low and High Serum Content (LC and HC, Respectively)[a]

				% of total	
av mass (Da)	accession number	gene name	protein name	LC	HC
30778	P02647	APOA1	apolipoprotein A-I	17.9	7.0
59578	P04196	HRG	histidine-rich glycoprotein	5.4	9.5
14747	P35542	SAA4	serum amyloid A-4 protein	4.4	2.7
36154	P02649	APOE	apolipoprotein E	3.9	3.2
11175	P02652	APOA2	apolipoprotein A-II	3.2	1.9
515611	P04114	APOB	apolipoprotein B-100	2.6	2.2
46737	P01009	A1AT	alpha-1-antitrypsin	1.7	1.5
39731	P27169	PON1	serum paraoxonase/ arylesterase 1	1.5	0.9
45399	P06727	APOA4	apolipoprotein A-IV	1.5	1.0
15887	P02766	TTHY	transthyretin	1.3	1.5
69367	P02768	ALBU	serum albumin	1.3	1.3
43974	O14791	APOL1	apolipoprotein L1	1.3	0.8
11765	P01834	IGKC	immunoglobulin kappa constant	1.2	1.2
13532	P0DJI8	SAA1	serum amyloid A-1 protein	1.2	0.7
10852	P02656	APOC3	apolipoprotein C-III	1.0	0.5
			total % top 15 proteins	49.5	35.8

[a]The corona formed on 300 μg/mL silica nanoparticles dispersed in 12 and 62 mg/mL human serum (low serum corona, LC, and high serum corona, HC, respectively) was prepared and isolated as described in the Methods. Thus, the corona proteins were identified by mass spectrometry, and their relative abundance over total (% of total) was quantified (see Methods for details). The table shows the relative abundance of the top 15 proteins identified in the two conditions.

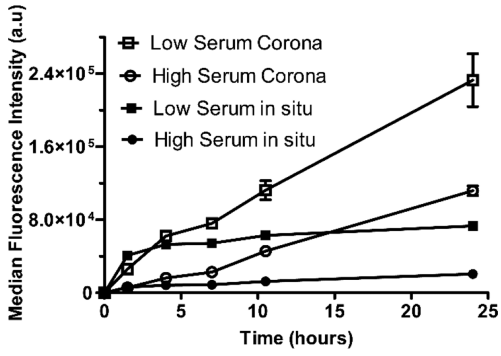

Figure 2. Uptake kinetics of 50 nm red silica nanoparticles in the presence of low and high human serum and the respective corona−nanoparticle complexes. HeLa cells were exposed to 100 μg/mL nanoparticles in a low or high amount of human serum *in situ* (4 and 20 mg/mL, respectively, with excess free proteins left in solution) or to the corresponding corona−nanoparticle complexes formed at the same nanoparticle to protein ratio, after removal of the free proteins in excess (see Methods for details). The results are the average and standard deviation over three replicates of the median cell fluorescence intensities obtained by flow cytometry.

DOI: 10.1021/acsnano.9b03824
ACS Nano 2019, 13, 11107−11121

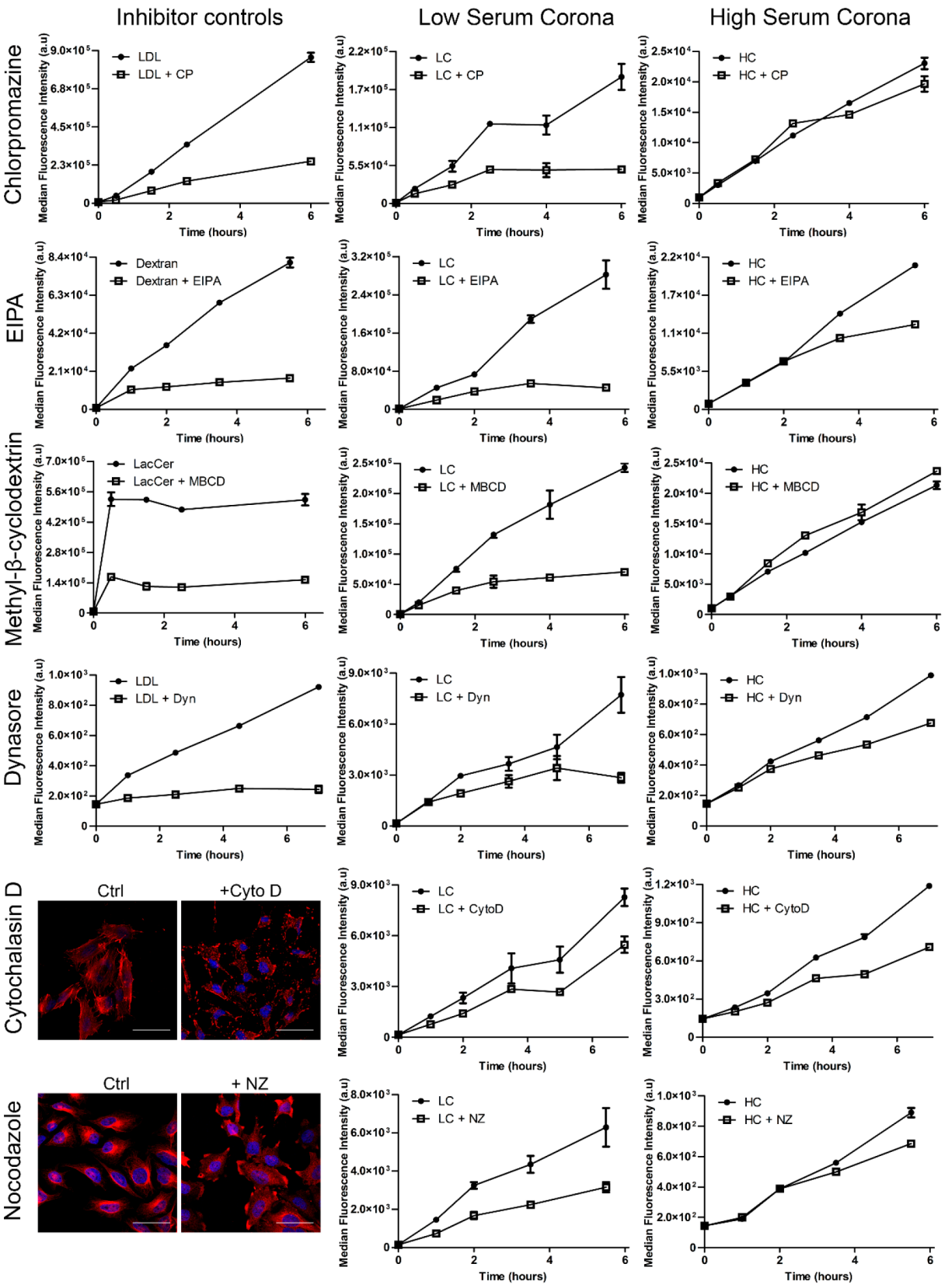

Figure 3. Characterization of the uptake mechanisms of the corona−nanoparticle complexes formed on 50 nm silica in low and high amounts of serum. Briefly, the corona−nanoparticle complexes formed on 300 μg/mL nanoparticles in MEM supplemented with 12 mg/mL (low-serum corona, LC, middle panels) or 62 mg/mL (high-serum corona, HC, right panels) of human serum were isolated as described in the Methods and added to HeLa cells at a final nanoparticle concentration of 100 μg/mL in serum-free medium, in the presence or absence of 100 μM EIPA, 10 μg/mL chlorpromazine (CP), 2.5 mg/mL methyl-β-cyclodextrin (MBCD), 25 μg/mL dynasore (Dyn), 2.5 μg/mL cytochalasin D (CytoD), or 5 μM nocodazole (NZ). For each inhibitor, the left panels show the corresponding controls of drug efficacy, with HeLa cells exposed to 2 μg/mL Dil-LDL in serum-free MEM as control for chlorpromazine and dynasore, 250 μg/mL 10 kDa TRITC

DOI: 10.1021/acsnano.9b03824
ACS Nano 2019, 13, 11107−11121

Figure 3. continued

dextran in complete MEM as control for EIPA, and 1 μM LacCer in serum-free MEM for methyl-β-cyclodextrin. Uptake kinetics were obtained by flow cytometry, and the results are the average and standard deviation over three replicates of the median cell fluorescence intensities of cells exposed to control markers or corona complexes with or without the different inhibitors. Immunostaining of actin and tubulin was used to confirm efficacy of cytochalasin D and nocodazole, respectively (see Methods for details). In the confocal fluorescence images: blue DAPI-stained nuclei and red-stained actin or tubulin. Scale bar: 100 μm.

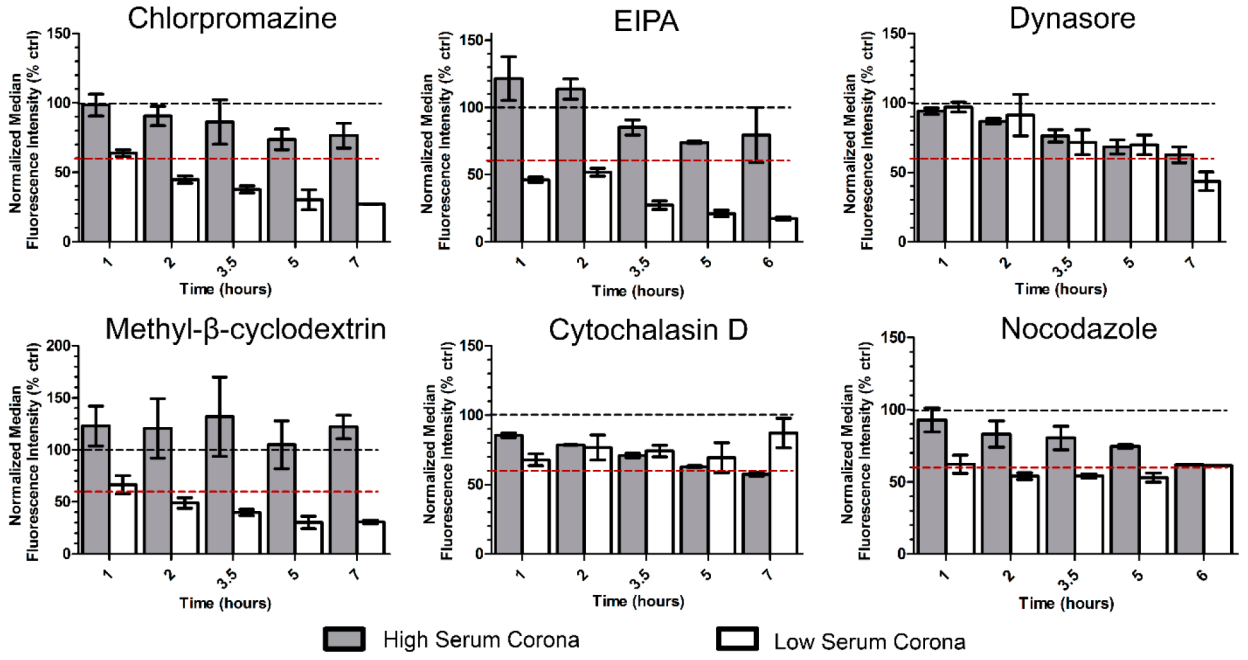

Figure 4. Overview of the effects of transport inhibitors on the uptake of the corona–nanoparticle complexes formed on 50 nm silica in low and high amounts of serum. Briefly, the corona complexes formed on 300 μg/mL nanoparticles in MEM supplemented with 12 mg/mL (low-serum corona) or 62 mg/mL (high-serum corona) of human serum were isolated as described in the Methods and incubated on HeLa cells at a final nanoparticle concentration of 100 μg/mL in serum-free medium, in the presence or absence of 100 μM EIPA, 10 μg/mL chlorpromazine, 2.5 mg/mL methyl-β-cyclodextrin (MβCD), 25 μg/mL dynasore, 2.5 μg/mL cytochalasin D, or 5 μM nocodazole. Data are normalized for the uptake in cells without inhibitors to show the inhibition efficacy. The results are the average and standard error of the median cell fluorescence intensities obtained in three independent experiments (with the exception of the last exposure time, 6 h, for cells exposed to nocodazole, and the last exposure time, 7 h, for cells exposed to for chlorpromazine in low-serum corona, which were performed once). The results of the individual experiments are shown in Supplementary Figure S3. A black dashed line and a red dashed line are included in each panel as a reference, at 100% and 60% uptake, respectively (with 60% uptake shown as an indicative threshold for inhibition efficacy).

serum the uptake efficiency was lower for the complexes formed at higher serum content. Quantification by fluorescence of the nanoparticles recovered after corona isolation confirmed that this was not simply due to loss of nanoparticles in the isolation procedure (Supplementary Table S1).

Confocal fluorescence imaging confirmed uptake of the corona–nanoparticle complexes formed in both low and high serum and—as observed for most nanomaterials[4,43,44]—accumulation in the lysosomes (Supplementary Figure S2).

Uptake Mechanisms of Low- and High-Serum Corona–Nanoparticle Complexes. In order to characterize the mechanisms of uptake of the different corona–nanoparticle complexes, common pharmacological inhibitors of endocytosis were used. These compounds are often used to study transport into cells, given their fast action and apparent ease of use.[41,42,45−48] However, due to their toxicity and limits connected to their mechanism of action, stringent controls are needed in order to verify their efficacy and set up protocols specific to the cells and conditions applied. We previously performed an extensive study on these aspects and carefully optimized their use on HeLa cells, in order to demonstrate their efficacy and minimize their toxicity.[49] The same conditions were applied for this study. There, we also found that the presence of serum can strongly limit the efficacy of some of these compounds. Thus, by using isolated corona complexes in serum-free conditions, we ensured optimal efficacy of all the inhibitors. Moreover, we performed time-resolved uptake studies in order to follow the kinetics of the process. Time-resolved studies allowed us to rule out the contribution of potential nanoparticles adhering outside cells, which can confuse uptake results at a single exposure time, especially when short.[50]

A panel of six different inhibitors was used. Figure 3 shows one representative example of the kinetics of uptake of corona–nanoparticle complexes formed in low and high amounts of serum (central and right panels) in the presence or absence of each of the different inhibitors. In every experiment and for each compound, a control to confirm inhibitor efficacy was also included (Figure 3, left panels). These results, together with two other independent replicates, are shown in Supplementary Figure S3 after normalization for the uptake in cells without inhibitors. Their normalized average

DOI: 10.1021/acsnano.9b03824
ACS Nano 2019, 13, 11107−11121

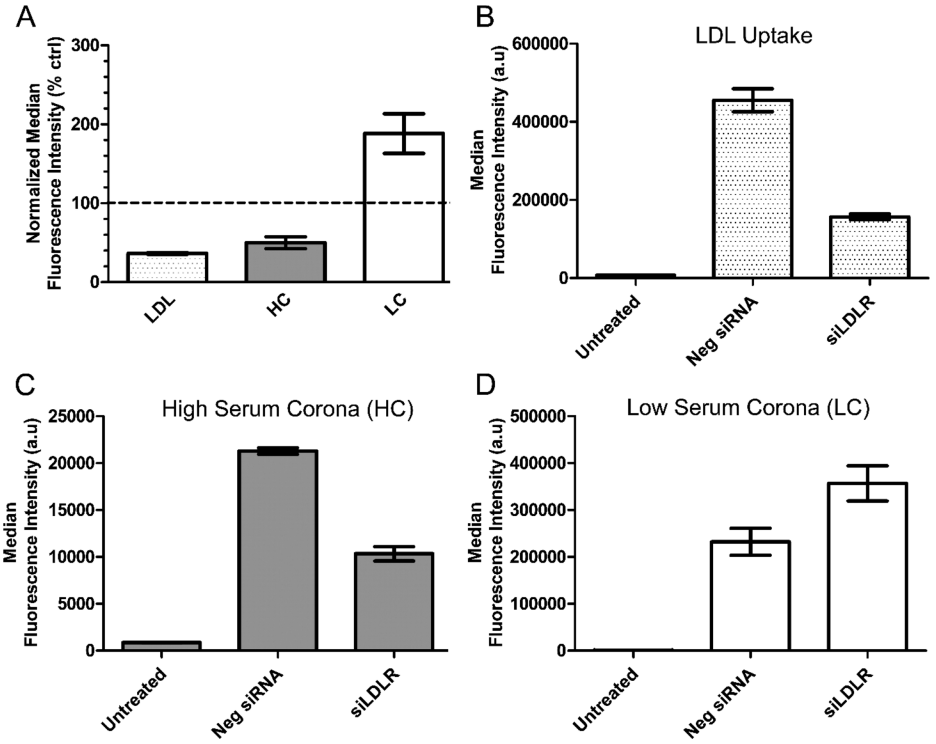

Figure 5. Involvement of the LDL receptor (LDLR) in the uptake of the corona−nanoparticle complexes formed on 50 nm silica in low and high amounts of serum. Briefly, the expression of the LDL receptor was silenced as described in the Methods (siLDLR). Cells silenced with a scramble siRNA were used as control (Neg siRNA). Then, the corona−nanoparticle complexes formed on 300 μg/mL nanoparticles in MEM supplemented with 12 mg/mL (LC, low-serum corona) or 62 mg/mL (HC, high-serum corona) of human serum were isolated as described in the Methods and incubated on HeLa cells at a final nanoparticle concentration of 100 μg/mL in serum-free medium for 14 h. The uptake of 1 μg/mL Dil-labeled LDL after 4.5 h exposure was measured to confirm silencing efficacy. (A) Uptake of LDL and HC or LC complexes on cells silenced for the LDL receptor, normalized by the uptake in control cells silenced with a scrambled siRNA. The results are the average and standard error of the median cell fluorescence intensity obtained by flow cytometry in three independent experiments. A black dashed line is included as a reference at 100% uptake. (B−D) Raw results (without normalization) of one representative experiment for the uptake of LDL (B), high-serum corona (C), and low-serum corona (D). The fluorescence of untreated control cells is included as a reference (Untreated). The data are the average and standard deviation over three replicates of the median cell fluorescence intensity obtained by flow cytometry.

is shown in Figure 4 as an overview of the inhibition efficacy (see Methods for details).

Chlorpromazine hydrochloride was used as a commonly used inhibitor of clathrin-mediated endocytosis,[41,46,47] one of the most relevant and characterized mechanisms of cellular uptake. It is generally believed that nanoparticles and drug carriers with sizes up to roughly 100 nm typically use clathrin-mediated endocytosis to enter cells.[41,51] Cells exposed to chlorpromazine showed up to 70% reduction of uptake of 1,1′-dioctadecyl-3,3,3′,3′-tetramethylindocarbocyanine perchlorate (Dil)-labeled LDL, known to enter cells *via* this mechanism,[52] confirming drug efficacy in the conditions applied. Interestingly, while for the complexes formed at low serum content uptake was substantially reduced in the presence of chlorpromazine (up to 75% reduction at the latest exposure time), only minor effects could be observed for the complexes formed at high serum content, with an uptake reduction between 0 and maximum 30% at different exposure times in different replicate experiments (Figures 3 and 4 and Supplementary Figure S3). This suggests that clathrin-mediated endocytosis is involved in the uptake of these nanoparticles only when they are added to cells in the presence of lower amounts of serum.

Next, EIPA (5-(*N*-ethyl-*N*-isopropyl)amiloride) was used as inhibitor of macropinocytosis.[53,54] This mechanism involves an actin-driven formation of membrane ruffles to engulf a portion of extracellular medium.[55] Several examples in the literature have suggested the involvement of this mechanism in the uptake of nanomedicines and nanoparticles.[48,56] EIPA efficacy on HeLa cells was confirmed using a fluorescent fluid phase marker, 10 kDa TRITC dextran; its uptake was reduced up to 80% after 5 h in the presence of EIPA. For the corona−nanoparticle complexes formed at low serum content, the uptake in the presence of EIPA was reduced from 50% to 80% at increasing exposure times, but for the complexes formed at high serum content only minor effects were observed (in the averaged results of Figure 4, between 0 and maximum 30% reduction at increasing exposure times). These results suggest that macropinocytosis is involved in the uptake of corona−nanoparticle complexes formed in the presence of a low amount of serum, with only minor effects at high-serum content.

The role of cholesterol in the uptake mechanism was assessed by using methyl-β-cyclodextrin, a compound that sequesters the cholesterol in the cell membrane, often used as an inhibitor of lipid-raft-mediated mechanisms. Methyl-β-cyclodextrin efficacy on HeLa cells was confirmed by measuring the uptake of a fluorescent sphingolipid, BODIPY FL C5-lactosylceramide/BSA complex (LacCer).[46,57] The results showed 70% reduction in LacCer uptake in the

DOI: 10.1021/acsnano.9b03824
ACS Nano 2019, 13, 11107−11121

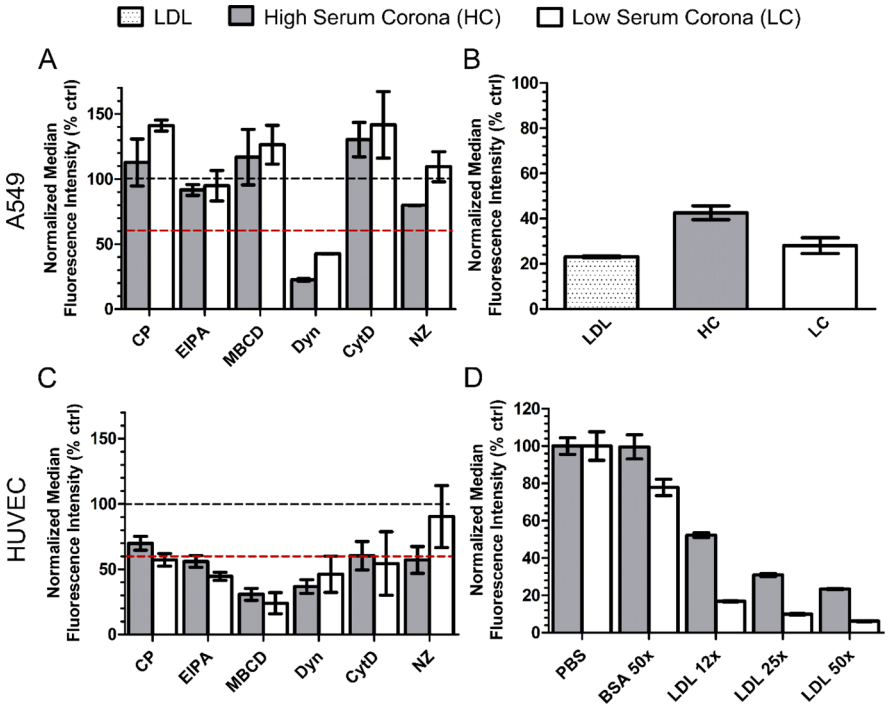

Figure 6. Characterization of the uptake mechanisms of the corona−nanoparticle complexes formed on 50 nm silica in low and high amounts of serum in A549 (A and B) and HUVEC (C and D) cells. Briefly, the corona−nanoparticle complexes formed on 300 μg/mL 50 nm silica nanoparticles in MEM supplemented with 12 mg/mL (LC, low serum corona) or 62 mg/mL (HC, high serum corona) of human serum were isolated as described in the Methods and incubated on cells at a final nanoparticle concentration of 100 μg/mL in serum-free medium. A549 (A) and HUVEC (C) cells were exposed for 6 h to the nanoparticles in the presence of chlorpromazine (CP), EIPA, methyl-β-cyclodextrin (MBCD), dynasore (Dyn), cytochalasin D (CytD), or nocodazole (NZ) (see Methods for details of concentrations for each cell line). Data are normalized for the uptake in cells without inhibitors. The results are the average and standard error of the median fluorescence intensity obtained in two independent experiments, which are shown in Supplementary Figure S5. A black dashed line and a red dashed line are included as a reference, at 100% and 60% uptake, respectively (with 60% uptake shown as an indicative threshold for inhibition efficacy). (B) Uptake of LC or HC corona−nanoparticle complexes (14 h exposure) and 1 μg/mL Dil-labeled LDL (4.5 h exposure) in A549 cells silenced for the LDL receptor (as described in the Methods). The results are the average and standard error of the median fluorescence intensity obtained in three independent experiments, normalized by the uptake in control cells silenced with a scrambled negative siRNA. (D) Uptake of LC or HC nanoparticle complexes by HUVEC in the presence of increasing amounts of unlabeled LDL (12× = 36 μg/mL; 24× = 73 μg/mL; 50× = 146 μg/mL, with respect to the number of nanoparticles added) or with bovine serum albumin (BSA 50× = 4,2 μg/mL) (14 h exposure). The results are the average and standard deviation over three replicates of the median cell fluorescence intensity obtained by flow cytometry, normalized by the uptake in cells exposed to the corona complexes in serum-free medium with the same volume of PBS added (PBS).

presence of methyl-β-cyclodextrin. Also in this case, nanoparticle uptake was strongly reduced for corona formed at low serum content (from 40% to 70% at increasing exposure times), whereas no effect was observed for the complexes formed at high serum content.

Next, dynasore was used to inhibit dynamin, a key protein for several pathways of endocytosis, including clathrin-mediated endocytosis and other dynamin-dependent mechanisms.[58,59] Dynamin mediates the scission of the cell membrane for the formation of the endosome. Dynasore efficacy on HeLa cells was confirmed by the strong reduction (75%) on the uptake of LDL in its presence. In cells exposed to dynasore, the uptake of the LC and HC complexes was reduced up to 30% in the first 5 h of exposure, while the inhibition seemed to increase to 60% and 40%, respectively, at the longest exposure time.

Finally, the role of the actin cytoskeleton and microtubules was studied using respectively cytochalasin D and nocodazole.[60,61] Actin has a predominant role for macropinocytosis to mediate the formation of membrane ruffles.[55] However, it is involved also in several other mechanisms, including clathrin-mediated endocytosis.[62,63] Disruption of actin and microtubules upon treatment with the inhibitors was confirmed by confocal microscopy using TRITC-phalloidin or an antibody against α-tubulin (Figures 3). For the LC complexes, only minor uptake reduction could be observed in the presence of cytochalasin D (on average a maximum 30% reduction). On the other hand, nocodazole had a strong effect on the uptake of these complexes (40−50% reduction at all exposure times). For the complexes formed in high serum instead, both cytochalasin D and nocodazole showed a similar trend, with the uptake reduction increasing up to 40% over time, possibly suggesting an actin and microtubule-driven mechanism at the longer exposure times.

Overall, the results suggest an involvement of multiple mechanisms in the two conditions. In the case of the corona−nanoparticle complexes formed in low amount of serum (white bars in Figure 4), clathrin-mediated endocytosis and macropinocytosis seem involved in the uptake, which also depends on cholesterol and microtubules. The limited effects observed with cytochalasin D, however, seem in contrast with the observed involvement of macropinocytosis. The time-resolved study also suggests a role for dynamin, mainly at longer exposure times.

DOI: 10.1021/acsnano.9b03824
ACS Nano 2019, 13, 11107−11121

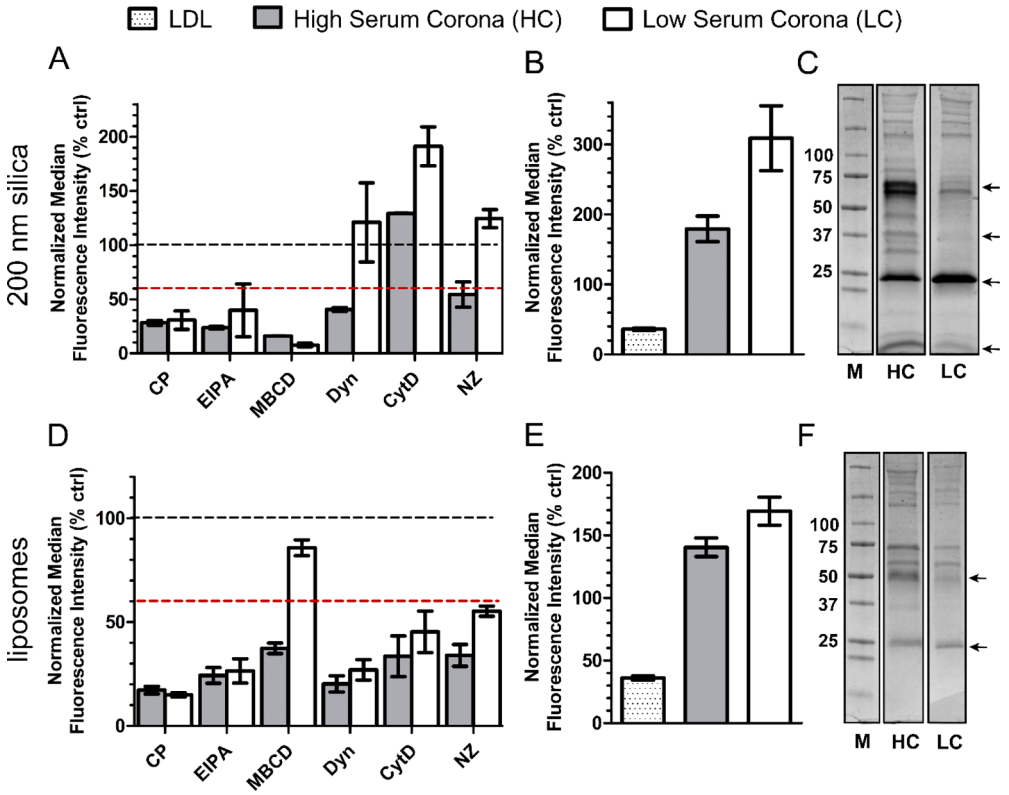

Figure 7. Characterization of the uptake mechanisms of the corona−nanoparticle complexes formed on 200 nm silica (A−C) and 100 nm liposomes (D−F) in low and high amount of serum in HeLa cells and corona composition. Briefly, the corona−nanoparticle complexes formed on 1200 μg/mL 200 nm silica nanoparticles or 300 μg/mL liposomes in MEM supplemented with 12 or 62 mg/mL human serum (low and high corona complexes, respectively, LC and HC complexes) were isolated as described in the Methods and incubated on cells in serum-free medium at a final nanoparticle concentration of 300 or 50 μg/mL, respectively. (A and D) Uptake in HeLa cells in the presence of chlorpromazine (CP), EIPA, methyl-β-cyclodextrin (MBCD), dynasore (Dyn), cytochalasin D (CytD), or nocodazole (NZ) (see Methods for details) after 7 h (A) or 5 h (D) exposure. Data are normalized for the uptake in cells without inhibitors. The results are the average and standard error of the median fluorescence intensity obtained in two independent experiments, which are shown in Supplementary Figure S7. A black dashed line and a red dashed line are included as a reference, at 100% and 60% uptake, respectively (with 60% uptake shown as an indicative threshold for inhibition efficacy). (B and E) Uptake of HC or LC complexes (14 h exposure) and 1 μg/mL DiI-labeled LDL (4.5 h exposure) in HeLa cells silenced for the LDL receptor (as described in the Methods). The results are the average and standard error of the median fluorescence intensity obtained in three independent experiments, normalized by the uptake in control cells silenced with a scrambled negative siRNA. (C and F) SDS-PAGE gel image of the proteins recovered on corona−nanoparticle complexes formed in low (LC) or high (HC) human serum content. The corona was prepared and isolated as described in the Methods. The gel images show that different bands were present in the corona formed in low and high serum content (arrows indicate some examples). M: molecular weight ladder.

Instead, in the case of corona−nanoparticle complexes formed in high amount of serum (gray bars in Figure 4) several differences were observed, and overall all inhibitors seemed to have minor effects in reducing nanoparticle uptake, perhaps increasing at the longer exposure times. One reason for this can be connected to the slower uptake kinetics for these complexes, even after corona isolation, making it harder to see clear effects on uptake when inhibitors are added (Figure 3, right panels). Unfortunately, these compounds cannot be used for much longer time, due to their intrinsic toxicity.[4,46] Nevertheless, the results suggested that, especially at the longest exposure times, HC uptake is partially dependent on dynamin, actin, and microtubules, however with effects never stronger than a 40% uptake reduction. On the other hand, as opposed to what was observed for LC complexes, clearly clathrin-mediated endocytosis, macropinocytosis, and cholesterol did not appear to be involved in the uptake of these nanoparticles when corona was formed at high serum content.

As a next step, we investigated the potential mechanisms beyond the observed differences. We hypothesized that different coronas are recognized differently by cell receptors, and this may lead to activation of different uptake mechanisms. To test this hypothesis, we used RNA interference to selectively shut down the expression of the LDL receptor and test its involvement in the recognition of the corona complexes in the two conditions (Figure 5). It was previously shown that in A549 lung epithelial cells the uptake of 100 nm silica nanoparticles dispersed in human serum was mediated by the recognition of the apolipoprotein B-100 present in the corona by the LDL receptor.[10] For each experiment, silencing efficacy was confirmed by measuring the uptake of labeled LDL. The results confirmed that silencing the expression of the LDL receptor reduced LDL uptake by about 60% (Figure 5A and B). Interestingly, even in HeLa cells and with the smaller 50 nm silica nanoparticles used for this study, silencing the expression of the LDL receptor reduced the uptake of the corona complexes formed in higher serum amount (Figure 5A and C), confirming its involvement in the uptake of these nanoparticles also in HeLa cells. However, no reduction (rather a strong increase) was observed in the uptake of the

DOI: 10.1021/acsnano.9b03824
ACS Nano 2019, 13, 11107−11121

corona complexes formed in low serum (Figure 5A and D). This suggests that, in agreement with our hypothesis, the different coronas formed on the 50 nm silica are recognized differently by the LDL receptor, and this, in turns, leads to the activation of different pathways for their internalization, as we observed (Figures 3 and 4).

It is interesting to notice that, in our system, the mass spectrometry results showed that apolipoprotein B-100, the major ligand of this receptor, was present in both coronas and in comparable amounts (Table 1). This indicates that the presence of certain proteins in the corona, alone, does not necessarily imply recognition by the corresponding cell receptors for nanoparticle internalization. Similarly, it is also most likely that other receptors, not investigated here, are involved in the two cases.

Next, we tested our hypothesis on other common cell models, namely, human lung epithelial cancer cells (A549) and primary HUVEC. Also for these cells, the conditions for using the panel of inhibitors were optimized in order to exclude toxicity and confirm drug efficacy (Supplementary Figures S4 and S5). Since different cell types express different cell receptors on the plasma membrane and uptake mechanisms are also differently active, we expected some differences in the way 50 nm silica nanoparticles were internalized by these cells. Indeed, the results showed that the effects of the inhibitors on the uptake of the HC and LC complexes were different in A549 cells and HUVEC (Figure 6) and with respect to what is observed in HeLa cells (Figure 4). In A549 cells overall the effects of the inhibitors on nanoparticle uptake were minor, with the exception of dynasore, which suggested a clear role for dynamin in the mechanisms involved in the uptake of both HC and LC complexes (Figure 6A and Supplementary Figure S5 for experiment replicates). In HUVEC most of the inhibitors reduced the uptake of nanoparticles, but no major differences between the two corona conditions were observed (Figure 6C and Supplementary Figure S5). These results suggest that in A549 cells and HUVEC similar mechanisms are involved in the uptake of the corona complexes formed in low and high amounts of serum. We then tested the involvement of the LDL receptor in all conditions. Interestingly, in A549 cells, as opposed to what was observed in HeLa cells, silencing the expression of the LDL receptor led to a strong reduction in the uptake of both the HC and LC complexes (Figure 6B). For the HUVEC, given the poor silencing efficacy in primary cells, LDL was added to the cells together with the corona−nanoparticle complexes in order to assess potential competition for the LDL receptor (Figure 6D). Although not as specific as silencing, adding increasing concentrations of unlabeled LDL caused a progressive reduction of the uptake of both the HC and LC complexes (the same was not observed when bovine serum albumin (BSA) was added, as a control), suggesting that the LDL receptor is involved in their internalization, possibly together with other LDL receptors, for which LDL could also compete.

Understanding all the factors controlling corona recognition by cell receptors and how these change in different cells remains a central challenge for the field, far beyond the scope of this paper. Nevertheless, these results suggest that when the same receptor is engaged (in this particular example, the LDL receptor), the same mechanisms are involved in the following internalization. This confirms the hypothesis that the initial recognition of corona proteins by specific cell receptors can affect the mechanisms of internalization.

As a final step, we performed similar experiments using other nanoparticles of different sizes and materials. For this purpose, we selected larger silica nanoparticles of 200 nm in diameter and 100 nm DOPG−cholesterol liposomes, as an example closer to the materials used in nanomedicine. Also with these nanoparticles, different coronas were formed by incubation with two different amounts of serum, followed by isolation of the corona−nanoparticle complexes by centrifugation and—in the case of the liposomes—size exclusion chromatography (see Methods for details). DLS characterization showed that for both materials good dispersions of the isolated corona−nanoparticles complexes could be obtained in both serum conditions (Supplementary Table S3 and Supplementary Figure S6). For the 200 nm silica, this was further confirmed by DCS and nanoparticle tracking analysis (NTA) (also in Supplementary Figure S6). SDS-PAGE showed that with both nanoparticles dispersion in different serum concentrations led to the adsorption of different proteins on their surface (Figure 7C and F, with arrows to show some examples of bands with different intensities in the two conditions).

Then, the panel of transport inhibitors was used to characterize the mechanisms of uptake in HeLa cells. The results showed that, as expected, different mechanisms were involved in the uptake of 200 nm silica and of the liposomes (Figure 7A and D, respectively, and Supplementary Figure S7 for experiment replicates), with respect to what was observed for the 50 nm silica (Figure 4).

Interestingly, as observed for the 50 nm silica, also for the 200 nm silica different mechanisms were involved in the uptake of corona−nanoparticle complexes formed in low and high serum amounts, the latter involving dynamin and microtubules (Figure 7A). This is a further confirmation that the corona composition can affect the mechanisms cells use to internalize nanoparticles.

In the case of the liposomes, instead, for most inhibitors no major differences were found in the two conditions. However, cholesterol depletion reduced the uptake of HC complexes by 60%, with only minor effects for LC ones (Figure 7D), confirming once more effects of corona composition on the uptake mechanisms.

As a final test, we assessed the involvement of the LDL receptor in the uptake of these nanoparticles. The results showed that for both nanoparticles and the different corona complexes silencing the expression of the LDL receptor did not affect uptake (Figure 7B and E). This indicates that in the case of these two nanoparticles other receptors are involved in the uptake. Further studies are required to identify all receptors involved in each case, including for the 50 nm silica, for which additional ones are likely to be involved, together with the LDL receptor.

In conclusion, the results presented indicate that the same nanoparticles can enter cells *via* different mechanisms when coated by coronas of different composition following dispersion in different protein contents. Changing protein concentration can also affect nanoparticle stability and, as a consequence of that, the following interactions with cells.[37−39] Indeed, in the case of the 50 nm silica, the presence of small agglomerates observed by DCS at lower serum content (Figure 1A) may contribute in part to some of the differences observed on HeLa cells in the uptake mechanisms of the LC and HC complexes (Figure 4). However, differences in uptake mechanisms were observed also with liposomes and 200 nm silica (Figure 7), for which characterization clearly showed that

DOI: 10.1021/acsnano.9b03824
ACS Nano 2019, 13, 11107−11121

homogeneous dispersions of isolated corona−nanoparticle complexes were obtained (Supplementary Figure S6). This excludes that the observed differences in uptake mechanisms are solely due to differences in nanoparticle stability and further confirms the hypothesis that corona composition can affect the mechanisms cells use to internalize nanoparticles.

CONCLUSIONS

So far, most studies on the mechanisms nanoparticles use to enter cells have adopted either serum-free conditions or dispersion in standard cell culture medium supplemented with a low amount of (bovine) serum. Serum is added to cell cultures simply for providing nutrients to cells. However, the presence of biological fluids has much more profound effects on the interactions of nanosized objects with cells, due to the adsorption of molecules on their surface and corona formation.[7] Cell receptors can recognize and engage with such corona proteins, and overall it is known that this layer strongly affects the subsequent interactions with cells.[10]

Given that corona proteins can be recognized by specific cell receptors, it comes natural to wonder whether this layer can also affect the mechanisms cells use to internalize nanosized objects. Recent works have shown that the presence or absence of a corona has an impact on the mechanisms cells use to internalize nanosized materials.[64,65] However, it is not known whether the corona composition (as opposed to simply the presence of a corona) also matters. This is of particular importance given that the same nanoparticles can form very different coronas depending on the biological fluid in which they are applied (thus the exposure route or, for nanomedicines, the administration route) and also on its concentration.[7,66] The implications can be profound. For instance, *in vivo,* nanoparticles in blood encounter much higher serum concentrations than what is usually applied in *in vitro* studies (passivating nanomedicines by exposure to serum prior to their administration *in vivo* may be considered in the future as an approach to try to control uncertainties related to changes in corona composition). Indeed, our results suggest that the corona composition can affect the initial recognition by cell receptors and, as a result, the same nanoparticle can be internalized by cells using different mechanisms when different coronas are formed. Potential subtle differences in nanoparticle stability for different coronas could also contribute in part to similar differences and should also be considered.

Another interesting observation is that nanoparticle uptake is lower at higher serum content. Similar observations were already reported for experiments where the excess proteins were left *in situ*,[12,67] possibly due to competition with the corona proteins for the same receptors.[10] However, here lower uptake was observed also after corona isolation and removal of excess free proteins. The lower uptake could be related to specific differences in corona composition. For instance, a study on macrophages suggested that the presence of histidine-rich glycoprotein in the corona is associated with a decreased uptake.[68] Here, similarly, the observed higher abundance of this protein in the corona formed at higher serum content could be one of the factors contributing to their lower uptake. Further studies are necessary to fully demonstrate similar effects connected to the relative abundance of individual proteins in the corona.

Next to this, the results suggest that multiple uptake mechanisms seem involved at the same time in the uptake of nanoparticles. It has been previously hypothesized that, within a sample, multiple subpopulations of different coronas may be formed,[7] and this could explain—at least in part—the observed co-presence of different uptake mechanisms. More subtle changes of corona composition over time and during exposure to cells could also explain this observation. Further studies are required to fully characterize the molecular details of the mechanisms involved in each case, possibly combining the use of transport inhibitors and RNA interference with other methods, such as the use of genetically modified cells.

Overall, these results clearly highlight the importance of defining what the "correct corona" is for each nanomedicine (or nanoparticle) when investigating its behavior on cells. For instance, for nanomedicines administered by injection, not only higher serum content but also other factors likely to affect corona composition should be considered, such as the presence of blood flow and the more complex composition of plasma *in vivo* (as opposed to the serum used here).[13,36] Similar considerations should also be applied to nanomedicines administered *via* different routes, for instance inhaled or ingested nanomedicines, for which a serum corona may be not relevant. Additionally, other more complex factors such as the evolution of corona composition over time and changes due to the interaction with secreted cellular biomolecules may also affect the uptake mechanisms on cells.[21,22,29,30]

Finally, while we could partially resolve the role of a particular receptor, here the LDL receptor, in mediating nanoparticle uptake in the different conditions tested, it is likely that many other receptors are involved, depending on the cell type, the nanoparticle, and the corona. Much more work will be required in this field to fully disentangle which epitopes are exposed on the outer surface of the corona and may be accessible for recognition by cells. Some first works have started to address this aspect and have illustrated its complexity.[17,69] Nevertheless, the phenomenon reported has profound implications for the field, and it is rather surprising to discover that this acquired layer can have such deep implications in the way cells process nanomaterials.

METHODS

Cell Culture. HeLa cells (ATCC CCL-2) and adenocarcinomic human alveolar basal epithelial cells (A549) (ATCC CCL-185) were cultured at 37 °C, 5% CO_2 in complete cell culture medium (cMEM) consisting of MEM (Gibco ThermoFisher Scientific) supplemented with 10% v/v fetal bovine serum (FBS, Gibco ThermoFisher Scientific). All experiments were performed with cells cultured for no longer than 20 passages after defrosting. Cells were tested monthly to exclude mycoplasma infection. HUVEC from pooled donors (LONZA) were cultured at 37 °C, 5% CO_2 in endothelial cell growth medium (Endothelial Cell Growth Medium 2, Promocell). In order to limit cell senescence and loss of the primary cell characteristics, experiments were performed using HUVEC from passage 2 to maximum 7. The medium was refreshed every 48 h.

Nanoparticle Characterization by DLS. Fluorescently labeled 50 and 200 nm silica nanoparticles (SiO_2) were purchased from Kisker Biotech. Nanoparticles were labeled by the manufacturer during polymerization using a fluorescent monomer with excitation and emission of 569/585 nm, respectively. Liposomes labeled with Dil dye with excitation and emission of 549/565 nm, respectively, were prepared as described below. Nanoparticle stability was assessed by measuring the particle hydrodynamic diameter by DLS using a Malvern Zetasizer Nano ZS (Malvern Instruments Ltd.) using disposable capillary cells (Malvern). The same instrument was used to measure nanoparticle zeta potential. Briefly, 100 μg/mL 50 and 200 nm silica and 300 μg/mL liposomes were dispersed in 1 mL of dH_2O

DOI: 10.1021/acsnano.9b03824
ACS Nano 2019, 13, 11107−11121

or PBS. Silica nanoparticles of 50 nm were also dispersed in MEM supplemented with 4 or 20 mg/mL pooled human serum (TCS BioSciences Ltd.). Additionally, the nanoparticle−corona complexes of 50 and 200 nm silica and of liposomes formed as described below were also characterized after isolation and dispersion in serum-free MEM at the same final concentration as applied on cells. In all cases, for each sample, at least three measurements of five runs each were performed.

Differential Centrifugal Sedimentation. Differential centrifugal sedimentation was performed using a CPS disc centrifuge model DC24000 (CPS Instruments Inc.) with an 8−24% sucrose gradient using water as the aqueous component (Merck) and a rotation speed of 18 000 rpm. Each particle size measurement was calibrated using 100 μL of a PVC standard with a nominal diameter of 0.237 μm (CPS Instruments Inc.). A 200 μL amount of 1 mg/mL silica nanoparticle dispersions in PBS or of the corona complexes formed as described below was injected. Two (200 nm silica) to three (50 nm silica) independent repetitions from separate corona−nanoparticle complex preparations were performed.

Nanoparticle Tracking Analysis. The corona complexes formed on 200 nm silica nanoparticle were characterized by nanoparticle tracking analysis using a ZetaView TWIN instrument (Particle Metrix). All samples were diluted in PBS to a final volume of 1 mL. Optimal measurement concentrations were found by pretesting the particle per frame value (100−200 particles/frame) and were typically a dilution of 1:10 000 from 1 mg/mL corona complexes or nanoparticles in PBS. For each sample, three technical replicates of one cycle were performed by scanning 11 cell positions each and capturing 60 frames per position (video setting: medium) under the following settings: focus, autofocus; camera sensitivity, 75.0; shutter, 100; scattering intensity, between 4 and 7; cell temperature, 25 °C. After capture, the videos were analyzed by the built-in ZetaView Software 8.05.05 with specific analysis parameters, which are a maximum particle size of 1000, a minimum particle size of 5, and a minimum particle brightness of 50. Two independent measurements on separate corona−nanoparticle complex preparations were performed.

Liposome Preparation and Characterization. Liposomes were prepared by thin lipid film hydration, followed by freeze−thaw cycles and extrusion. Briefly, DOPG, cholesterol (Avanti Polar Lipids), and the lipophilic dye DiI (Sigma-Aldrich) in a molar ratio of 2.5:1:0.005 were dissolved and mixed in chloroform. The organic solvent was evaporated with dry nitrogen for 30 min and under vacuum overnight. Then, the lipid film was hydrated with PBS to produce large multilamellar liposomes at a final concentration of 10 mg/mL lipids. Small unilamellar liposomes were obtained by eight freeze and thaw cycles in liquid nitrogen and warm water and 21 extrusions through a 0.1 μm polycarbonate membrane using the Avanti mini-extruder (Avanti Polar Lipids). Zeta spin desalting columns (7K MWCO, from ThermoFisher Scientific) were used to remove potential free DiI. Liposomes were stored at 4 °C and used for a maximum of one month after preparation. The final lipid concentration was quantified *via* Stewart assay.[70] For this, a ferrothiocyanate reagent was prepared first by dissolving 27 mg of ferric chloride hexahydrate (Sigma-Aldrich) and 30.4 mg of ammonium thiocyanate (Sigma-Aldrich) in 1 mL of Milli-Q water. Then, 10 μL of liposomes was mixed with 1 mL of chloroform and 1 mL of ferrothiocyanate reagent, followed by 1 min vortex and 10 min centrifugation at 300*g*. The organic phase was transferred to a quartz cuvette, and the absorbance was measured at 470 nm with a Unicam UV500 spectrophotometer (Unicam Instruments). The lipid concentration was calculated according to a standard curve.

Silica Corona−Nanoparticle Complex Preparation and Characterization. Corona−nanoparticle complexes were formed and isolated before incubation on cells and characterization. Briefly, 300 μg/mL 50 nm or 1200 μg/mL 200 nm silica nanoparticles were dispersed in MEM containing roughly 62 mg/mL (HC nanoparticles) or 12 mg/mL (LC nanoparticles) pooled human serum (TCS BioSciences) diluted in PBS at 37 °C under continuous shaking (250 rpm). After 1 h of incubation the dispersion was centrifuged for 1 h at 15 °C (for 50 nm silica) or 30 min (for 200 nm silica) at 16000*g* in order to pellet the corona−nanoparticle complexes. The supernatant containing unbound serum was collected, and its fluorescence at 600 nm after excitation at 550 nm measured with a SpectraMax Gemini XPS microplate spectrofluorometer (Molecular Devices), together with that of the resuspended pellet in order to verify that no nanoparticles were left in solution and all of them were recovered in the pellet (see Supplementary Table S1 for details). The pellet containing corona−nanoparticle complexes was resuspended to 1 mg/mL nanoparticle in PBS by careful pipeting. For cell experiments with isolated corona−nanoparticle complexes, for 50 nm silica nanoparticles the complexes were further diluted in serum-free MEM to a final concentration of 100 μg/mL and then added to cells. For 200 nm silica, the corona−nanoparticle complexes were diluted in serum-free MEM to a final concentration of 300 μg/mL for 7 h of exposure on cells for uptake studies with the inhibitors and 25 μg/mL for 14 h of exposure for silencing experiments. For SDS PAGE and mass spectrometry analysis, instead, the corona−nanoparticle complexes were washed in 1 mL of PBS and centrifuged again at 16000*g* for 1 h for 50 nm silica (or 30 min, for 200 nm silica) for a total of four centrifugations, in order to isolate hard corona-coated nanoparticles. The final amount of nanoparticles present in the pellet after four washing steps was quantified again as above with a spectrofluorometer. Afterward, the corona−nanoparticle complexes were resuspended in gel loading buffer, boiled 5 min at 95 °C, and loaded into a 10% polyacrylamide gel for SDS-PAGE. The complexes recovered were quantified by fluorescence measurement as described above, and the same amount of high and low corona−nanoparticle complexes were loaded in each well. After the electrophoretic run, the gel was incubated for 1 h with a solution containing 0.1% w/v Coomassie blue R-250 in a water/methanol/glacial acetic acid (5:4:1) solution and washed with Milli-Q water, and pictures were taken using a ChemiDoc XRS (Biorad).

For the isolation of the corona−nanoparticle complexes for differential centrifugal sedimentation and nanoparticle tracking analysis, the samples (prepared as described above) were spun down using a benchtop Eppendorf centrifuge (Sigma 3-30KS) for 40 min at 4 °C at 14000*g* (50 nm silica) or 15 min at 16000*g* (200 nm silica).

Corona−Liposome Complex Preparation and Characterization. Liposomes (300 μg/mL) were incubated with 12 or 62 mg/mL human serum at 37 °C, 250 rpm. After 1 h of incubation, size exclusion chromatography was used to separate the liposome−corona complexes from the unbound proteins. Briefly, 1 mL of sample was loaded on a 15 × 1.5 cm Sepharose CL-4B column (Sigma-Aldrich) equilibrated with PBS. The eluate was collected in fractions of 0.5 mL. The absorbance of each fraction was measured at 280 nm (for proteins) and 549 nm (for DiI) using a NanoDrop One Microvolume UV−vis spectrophotometer (ThermoFisher Scientific). The fractions containing the liposome−corona complexes were pooled together and concentrated by using an Amicon Ultra-15 centrifugal filter (30 kDa, Millipore) for 1 h at 1700*g*. The lipid concentration was measured by a Stewart assay, as described above, and the liposome−corona complexes were dispersed in serum-free MEM and incubated on cells at a final concentration of 50 μg/mL for 5 h for uptake studies with the inhibitors and for 14 h for silencing experiments. For SDS PAGE, the corona−liposome complexes were further concentrated and then resuspended in gel loading buffer, boiled 5 min at 95 °C, and loaded into a 10% polyacrylamide gel for SDS-PAGE. After the electrophoretic run, the gel was incubated for 1 h with a solution containing 0.1% w/v Coomassie blue R-250 (Sigma-Aldrich) in a water/methanol/glacial acetic acid (5:4:1) solution and washed with Milli-Q water, and pictures were taken using a ChemiDoc XRS (Biorad).

Mass Spectrometry Analysis. For mass spectrometry analysis, the protein content of the recovered 50 nm silica corona−nanoparticles complexes prepared as described above was quantified after four centrifugation and washing steps using a Pierce BCA protein assay kit (ThermoFisher) following the manufacturer's instructions. Then, corona−nanoparticle complexes were diluted in PBS in order to have the same protein concentration for all samples. Samples were

DOI: 10.1021/acsnano.9b03824
ACS Nano 2019, 13, 11107−11121

incubated with the same volume of 0.1% Rapigest (Waters Chromatography B.V.), an MS-compatible surfactant used to enhance enzymatic digestion of proteins. Afterward, samples were incubated for 3 h at 37 °C with 40 μL of a solution of 400 ng of sequencing grade modified trypsin (Promega Corporation) resuspended in 0.1% Rapigest, to allow protein digestion. Samples were shaken every hour during digestion. The digestion reaction was stopped by adding 10 μL of 75% v/v acetonitrile and 25% of a solution of 5% v/v formic acid in water. The nanoparticles and digested peptides were loaded in SPE (solid phase extraction) GracePure columns (W. R. Grace & Co.). Columns were first equilibrated by adding twice 1 mL of 0.1% v/v formic acid in acetonitrile and then twice 1 mL of 0.1% v/v formic acid in water. Then 900 μL of 0.1% v/v formic acid in water was added to the samples, which were subsequently loaded in the columns. Samples were washed twice with 1 mL of 0.1% v/v formic acid in water and then eluted by adding twice 400 μL of 50% v/v acetonitrile + 0.1% v/v formic acid. The eluted sample was spun down for 5 min at 16 100 rcf in order to pellet down the remaining nanoparticles. The supernatant containing the peptides was collected and dried using a speed vacuum for about 2 h. Afterward, samples were resuspended in 75 μL of 0.1% formic acid in water, and 2 μL samples were loaded into a Q Exactive Plus hybrid quadrupole–orbitrap mass spectrometer (ThermoFisher) using Acclaim PepMap 100 C18 LC columns (ThermoFisher). Samples were analyzed using the software PEAKS Studio 8.5 (Bioinformatics Solutions Inc.), and proteins identified using the manually reviewed UniProtKB/Swiss-Prot database. Only proteins identified by at least one unique peptide were included in the analysis. Spectral counts were normalized by the molecular weight of the identified protein and the total normalized spectral counts used to calculate the relative abundance of each protein in the corona (% of total).

Uptake Studies with Pharmacological Inhibitors of Transport. HeLa, A549, and HUVEC cells were treated with pharmacological inhibitors in order to characterize the uptake mechanism of the corona–nanoparticle complexes formed in low and high serum content. The optimization of the incubation conditions of the inhibitors in HeLa cells has been described elsewhere.[49] Briefly, 50 000 cells/well were seeded in a 24-well plate (Greiner) 1 day before the experiments. For HUVEC, wells were precoated with 0.1 mg/mL cold rat-tail collagen type-I (Corning) for 1 h and washed three times with PBS before cell seeding. Cells were pretreated with the inhibitors for 10 min (or 20 min for nocodazole) in MEM or cMEM. The concentrations of inhibitors used in the present work are the following: 100 μM (HeLa), 40 μM (A549), or 50 μM (HUVEC) EIPA, 10 μg/mL (HeLa) or 5 μg/mL (A549, HUVEC) chlorpromazine hydrochloride, 2.5 mg/mL (HeLa), 2 mg/mL (A549), or 4 mg/mL (HUVEC) methyl-β-cyclodextrin, 25 μg/mL (HeLa), 50 μg/mL (A549), or 50 μg/mL (HUVEC) dynasore (all from Sigma-Aldrich), 5 μM (HeLa, A549) or 2.5 μM (HUVEC) nocodazole (Biovision), 2.5 μg/mL (HeLa, A549) or 0.5 μg/mL (HUVEC) cytochalasin D (ThermoFisher Scientific). Afterward, the corona–nanoparticles complexes were incubated on cells with or without the inhibitors. Drug efficacy was assessed in parallel for each experiment by measuring the uptake of markers of endocytosis, by light microscopy or by immunohistochemistry. As a control for chlorpromazine and dynasore, the uptake of 2 μg/mL fluorescently labeled low-density lipoprotein, Dil-LDL (ThermoFisher Scientific), dispersed in serum-free MEM was measured. As a control for methyl-β-cyclodextrin, the uptake of 1 μg/mL BODIPY LacCer (ThermoFisher Scientific) in serum-free MEM was measured. As a control for EIPA, the uptake of 250 μg/mL 10 kDa TRITC dextran (ThermoFisher Scientific) in cMEM was used.

Flow Cytometry Analysis. HeLa, A549, and HUVEC cells were incubated with red fluorescently labeled 50 nm silica nanoparticles, red fluorescently labeled 200 nm silica nanoparticles, Dil-labeled DOPG–cholesterol liposomes, BODIPY FL C5-LacCer, 10 kDa TRITC dextran, or Dil-LDL, and their uptake was measured by flow cytometry. After exposure, cells were washed with cMEM and twice with PBS to remove the excess nanoparticles and markers and minimize the eventual contribution of nanoparticles adhering outside cells.[46] Afterward, cells were harvested using 0.05% trypsin–EDTA for 5 min, centrifuged, resuspended in PBS, and measured immediately using a Cytoflex flow cytometer (Beckman Coulter) with a 488 or 561 nm laser. Data were analyzed using Flowjo software (Flowjo, LLC). Dead cells and cell doublets were excluded from the analysis by setting gates in the forward and side scattering double scatter plots. At least 20 000 cells were acquired for each sample, and each condition was repeated in triplicate. Results are expressed as the average of the median cell fluorescence intensity and standard deviation over the three technical replicates, unless otherwise stated.

Immunohistochemistry and Fluorescence Imaging. The efficacy of cytochalasin D and nocodazole on, respectively, actin or microtubule disruption and the uptake and distribution of 50 nm silica nanoparticles in HeLa cells was assessed by immunohistochemistry. A total of 50 000 cells/well HeLa cells were seeded in a 24-well plate in which glass coverslips were inserted. After 24 h, the corona complexes formed on 300 μg/mL 50 nm silica nanoparticles in MEM supplemented with 12 or 62 mg/mL human serum were isolated as described above and incubated at a concentration of 100 μg/mL in serum-free medium for 5 h. Then, cells were washed for 30 min in MEM supplemented with 10% FBS, in order to remove the excess of nanoparticles in the incubation medium and on the cell surface. Next, cells were washed with PBS and fixed by incubation in 4% formaldehyde for 15 min at room temperature, and the cell membrane was permeabilized by incubation in 0.1% saponin for 5 min. Then, HeLa cells treated with nocodazole were incubated for 1 h with a mouse primary antibody against human α-tubulin (Merck Millipore) followed by 1 h of incubation with a goat anti-mouse Alexa Fluor488 secondary antibody (ThermoFisher Scientific). Cells treated with cytochalasin D were incubated with TRITC-Phalloidin (Sigma-Aldrich), which selectively stains F-actin. Lysosomal staining was performed by incubating cells with a mouse primary antibody against LAMP-1 (clone H4A3, BD Biosciences) for 1 h, followed by 1 h of incubation with an Alexa Fluor 488 goat secondary anti-mouse antibody. Cells were washed three times with PBS after each antibody incubation and subsequently incubated for 5 min with a PBS solution containing 0.2 μg/mL 4′,6-diamidino-2-phenylindole (DAPI) for nuclear staining. Finally, the coverslips were mounted on glass slides using Mowiol 4-88 mounting medium (EMD Chemical, Inc.). Images were acquired using a Leica TCS SP8 confocal fluorescence microscope (Leica Microsystems) with a 63× objective, using a 405 nm laser for DAPI excitation, a 488 nm laser for Alexa Fluor488 secondary antibody, and a 552 nm laser for TRITC-Phalloidin. ImageJ software (http://www.fiji.sc) was used for image processing.

Silencing and Competition Experiments. In order to silence the expression of the LDL receptor in HeLa and A549 cells, oligofectamine (ThermoFisher) and Silencer Select siRNA (ThermoFisher) were used. Briefly, 13 000 cells/well were seeded in a 24-well plate (Greiner). Twenty-four hours after seeding, cells were washed in serum-free MEM for 20 min. Then, each well was incubated with 250 μL of a mix including 1 μL of oligofectamine, 10 pmol of siRNA, and Opti-MEM (ThermoFisher), prepared according to the manufacturer's instructions. A scrambled siRNA was used as a negative control (Neg siRNA). After 4 h, 125 μL of MEM supplemented with 30% v/v fetal bovine serum was added to each well, and cells were grown for a further 72 h at 37 °C, 5% CO_2. After a 72 h silencing, cells were exposed to the corona complexes or Dil-LDL as described above.

For competition experiments with HUVEC, 50 000 cells/well were seeded in a 24-well plate (Greiner) precoated with collagen as described above. Twenty-four hours after seeding, cells were exposed for 14 h to the corona complexes in serum-free MEM or medium containing increasing concentrations of unlabeled LDL (BioVision).

ASSOCIATED CONTENT

Supporting Information

The Supporting Information is available free of charge on the ACS Publications website at DOI: 10.1021/acsnano.9b03824.

Dispersion characterization, uptake results of independent replicate experiments, confocal microscopy images

DOI: 10.1021/acsnano.9b03824
ACS Nano 2019, 13, 11107–11121

of cells exposed to the corona-nanoparticle complexes and the optimization of the inhibitors on A549 cells and HUVEC (PDF)

Full results obtained by mass spectrometry for the identification of the proteins recovered in the corona formed on the silica nanoparticles in low and high serum content (XLSX)

AUTHOR INFORMATION

Corresponding Author

*E-mail: a.salvati@rug.nl.

ORCID

Valentina Francia: 0000-0003-4911-6832

Sarah Deville: 0000-0002-5615-8603

Anna Salvati: 0000-0002-9339-0161

Notes

The authors declare no competing financial interest.

ACKNOWLEDGMENTS

This work was funded by the European Research Council (ERC) under the European Union's Horizon 2020 Research and Innovation Programme under grant agreement no. 637614 (NanoPaths). A.S. kindly acknowledges the University of Groningen for additional funding (Rosalind Franklin Fellowship). S.D. was supported by a postdoctoral fellowship granted by the Research Foundation Flanders (FWO) and the Flemish Institute for Technological Research (VITO) under grant agreement 12S6517N. Financial support from the China Scholarship Council to K.Y. is also acknowledged. Mass spectrometry analysis was performed in the Interfaculty Mass Spectrometry Center of the University of Groningen (RUG) and University Medical Center Groningen (UMCG). The authors would like to thank H. Permentier and C. M. Jeronimus-Stratingh for technical help and suggestions for sample preparation for mass spectrometry.

REFERENCES

(1) Ferrari, M. Cancer Nanotechnology: Opportunities and Challenges. *Nat. Rev. Cancer* **2005**, *5*, 161−171.

(2) Chauhan, V. P.; Jain, R. K. Strategies for Advancing Cancer Nanomedicine. *Nat. Mater.* **2013**, *12*, 958−962.

(3) Shi, J.; Kantoff, P. W.; Wooster, R.; Farokhzad, O. C. Cancer Nanomedicine: Progress, Challenges and Opportunities. *Nat. Rev. Cancer* **2017**, *17*, 20−37.

(4) Iversen, T. G.; Skotland, T.; Sandvig, K. Endocytosis and Intracellular Transport of Nanoparticles: Present Knowledge and Need for Future Studies. *Nano Today* **2011**, *6*, 176−185.

(5) Editorial. Time to Deliver. *Nat. Biotechnol.* **2014**, *32*, 961.

(6) Farokhzad, O. C.; Langer, R. Impact of Nanotechnology on Drug Delivery. *ACS Nano* **2009**, *3*, 16−20.

(7) Monopoli, M. P.; Åberg, C.; Salvati, A.; Dawson, K. A. Biomolecular Coronas Provide the Biological Identity of Nanosized Materials. *Nat. Nanotechnol.* **2012**, *7*, 779−786.

(8) Nel, A. E.; Mädler, L.; Velegol, D.; Xia, T.; Hoek, E. M. V.; Somasundaran, P.; Klaessig, F.; Castranova, V.; Thompson, M. Understanding Biophysicochemical Interactions at the Nano-Bio Interface. *Nat. Mater.* **2009**, *8*, 543−557.

(9) Dobrovolskaia, M. A.; Shurin, M.; Shvedova, A. A. Current Understanding of Interactions Between Nanoparticles and the Immune System. *Toxicol. Appl. Pharmacol.* **2016**, *299*, 78−89.

(10) Lara, S.; Alnasser, F.; Polo, E.; Garry, D.; Lo Giudice, M. C.; Hristov, D. R.; Rocks, L.; Salvati, A.; Yan, Y.; Dawson, K. A. Identification of Receptor Binding to the Biomolecular Corona of Nanoparticles. *ACS Nano* **2017**, *11*, 1884−1893.

(11) Dai, Q.; Guo, J.; Yan, Y.; Ang, C. S.; Bertleff-Zieschang, N.; Caruso, F. Cell-Conditioned Protein Coronas on Engineered Particles Influence Immune Responses. *Biomacromolecules* **2017**, *18*, 431−439.

(12) Salvati, A.; Pitek, A. S.; Monopoli, M. P.; Prapainop, K.; Baldelli Bombelli, F.; Hristov, D. R.; Kelly, P. M.; Åberg, C.; Mahon, E.; Dawson, K. A. Transferrin-Functionalized Nanoparticles Lose Their Targeting Capabilities When a Biomolecule Corona Adsorbs on the Surface. *Nat. Nanotechnol.* **2013**, *8*, 137−143.

(13) Hadjidemetriou, M.; Al-Ahmady, Z.; Mazza, M.; Collins, R. F.; Dawson, K.; Kostarelos, K. *In Vivo* Biomolecule Corona around Blood-Circulating, Clinically Used and Antibody-Targeted Lipid Bilayer Nanoscale Vesicles. *ACS Nano* **2015**, *9*, 8142−8156.

(14) Pozzi, D.; Colapicchioni, V.; Caracciolo, G.; Piovesana, S.; Capriotti, A. L.; Palchetti, S.; De Grossi, S.; Riccioli, A.; Amenitsch, H.; Laganà, A. Effect of Polyethyleneglycol (PEG) Chain Length on the Bio−Nano-Interactions between PEGylated Lipid Nanoparticles and Biological Fluids: From Nanostructure to Uptake in Cancer Cells. *Nanoscale* **2014**, *6*, 2782−2792.

(15) Veronese, F. M.; Pasut, G. PEGylation, Successful Approach to Drug Delivery. *Drug Discovery Today* **2005**, *10*, 1451−1458.

(16) Greenwald, R. B.; Choe, Y. H.; McGuire, J.; Conover, C. D. Effective Drug Delivery by PEGylated Drug Conjugates. *Adv. Drug Delivery Rev.* **2003**, *55*, 217−250.

(17) Schöttler, S.; Becker, G.; Winzen, S.; Steinbach, T.; Mohr, K.; Landfester, K.; Mailänder, V.; Wurm, F. R. Protein Adsorption Is Required for Stealth Effect of Poly(Ethylene Glycol)- and Poly-(Phosphoester)-Coated Nanocarriers. *Nat. Nanotechnol.* **2016**, *11*, 372−377.

(18) Wagner, S.; Zensi, A.; Wien, S. L.; Tschickardt, S. E.; Maier, W.; Vogel, T.; Worek, F.; Pietrzik, C. U.; Kreuter, J.; von Briesen, H. Uptake Mechanism of ApoE-Modified Nanoparticles on Brain Capillary Endothelial Cells As a Blood-Brain Barrier Model. *PLoS One* **2012**, *7*, 3−9.

(19) Kah, J. C. Y.; Chen, J.; Zubieta, A.; Hamad-Schifferli, K. Exploiting the Protein Corona Around Gold Nanorods for Loading and Triggered Release. *ACS Nano* **2012**, *6*, 6730−6740.

(20) Caracciolo, G.; Cardarelli, F.; Pozzi, D.; Salomone, F.; Maccari, G.; Bardi, G.; Capriotti, A. L.; Cavaliere, C.; Papi, M.; Laganà, A. Selective Targeting Capability Acquired with a Protein Corona Adsorbed on the Surface of 1,2-Dioleoyl-3-Trimethylammonium Propane/Dna Nanoparticles. *ACS Appl. Mater. Interfaces* **2013**, *5*, 13171−13179.

(21) Tenzer, S.; Docter, D.; Kuharev, J.; Musyanovych, A.; Fetz, V.; Hecht, R.; Schlenk, F.; Fischer, D.; Kiouptsi, K.; Reinhardt, C.; Landfester, K.; Schild, H.; Maskos, M.; Knauer, S. K.; Stauber, R. H. Rapid Formation of Plasma Protein Corona Critically Affects Nanoparticle Pathophysiology. *Nat. Nanotechnol.* **2013**, *8*, 772−781.

(22) Casals, E.; Pfaller, T.; Duschl, A.; Oostingh, G. J.; Puntes, V. Time Evolution of Nanoparticle Protein Corona. *ACS Nano* **2010**, *4*, 3623−3632.

(23) Röcker, C.; Pötzl, M.; Zhang, F.; Parak, W. J.; Nienhaus, G. U. A Quantitative Fluorescence Study of Protein Monolayer Formation on Colloidal Nanoparticles. *Nat. Nanotechnol.* **2009**, *4*, 577−580.

(24) Cedervall, T.; Lynch, I.; Lindman, S.; Berggard, T.; Thulin, E.; Nilsson, H.; Dawson, K. A.; Linse, S. Understanding the Nanoparticle-Protein Corona Using Methods to Quantify Exchange Rates and Affinities of Proteins for Nanoparticles. *Proc. Natl. Acad. Sci. U. S. A.* **2007**, *104*, 2050−2055.

(25) Duan, X.; Li, Y. Physicochemical Characteristics of Nanoparticles Affect Circulation, Biodistribution, Cellular Internalization, and Trafficking. *Small* **2013**, *9*, 1521−1532.

(26) Lundqvist, M.; Stigler, J.; Elia, G.; Lynch, I.; Cedervall, T.; Dawson, K. a. Nanoparticle Size and Surface Properties Determine the Protein Corona with Possible Implications for Biological Impacts. *Proc. Natl. Acad. Sci. U. S. A.* **2008**, *105*, 14265−14270.

(27) Mirshafiee, V.; Kim, R.; Mahmoudi, M.; Kraft, M. L. The Importance of Selecting a Proper Biological Milieu for Protein Corona Analysis *In Vitro*: Human Plasma *Versus* Human Serum. *Int. J. Biochem. Cell Biol.* **2016**, *75*, 188−195.

DOI: 10.1021/acsnano.9b03824
ACS Nano 2019, 13, 11107−11121

(28) Monopoli, M. P.; Walczyk, D.; Campbell, A.; Elia, G.; Lynch, I.; Baldelli Bombelli, F.; Dawson, K. A. Physical-Chemical Aspects of Protein Corona : Relevance to *In Vitro* and *In Vivo* Biological Impacts of Nanoparticles. *J. Am. Chem. Soc.* **2011**, *133*, 2525−2534.
(29) Barrán-Berdón, A. L.; Pozzi, D.; Caracciolo, G.; Capriotti, A. L.; Caruso, G.; Cavaliere, C.; Riccioli, A.; Palchetti, S.; Laganaì, A. Time Evolution of Nanoparticle-Protein Corona in Human Plasma: Relevance for Targeted Drug Delivery. *Langmuir* **2013**, *29*, 6485−6494.
(30) Albanese, A.; Walkey, C. D.; Olsen, J. B.; Guo, H.; Emili, A.; Chan, W. C. W. Secreted Biomolecules Alter the Biological Identity and Cellular Interactions of Nanoparticles. *ACS Nano* **2014**, *8*, 5515−5526.
(31) Walkey, C. D.; Olsen, J. B.; Song, F.; Liu, R.; Guo, H.; Olsen, D. W. H.; Cohen, Y.; Emili, A.; Chan, W. C. W. Protein Corona Fingerprinting Predicts the Cellular Interaction of Gold and Silver Nanoparticles. *ACS Nano* **2014**, *8*, 2439−2455.
(32) Deng, Z. J.; Liang, M.; Monteiro, M.; Toth, I.; Minchin, R. F. Nanoparticle-Induced Unfolding of Fibrinogen Promotes Mac-1 Receptor Activation and Inflammation. *Nat. Nanotechnol.* **2011**, *6*, 39−44.
(33) Gilleron, J.; Querbes, W.; Zeigerer, A.; Borodovsky, A.; Marsico, G.; Schubert, U.; Manygoats, K.; Seifert, S.; Andree, C.; Stöter, M.; Epstein-Barash, H.; Zhang, L.; Koteliansky, V.; Fitzgerald, K.; Fava, E.; Bickle, M.; Kalaidzidis, Y.; Akinc, A.; Maier, M.; Zerial, M. Image-Based Analysis of Lipid Nanoparticle-Mediated SiRNA Delivery, Intracellular Trafficking and Endosomal Escape. *Nat. Biotechnol.* **2013**, *31*, 638−646.
(34) Walczyk, D.; Baldelli Bombelli, F.; Monopoli, M. P.; Lynch, I.; Dawson, K. A. What the Cell "Sees" in Bionanoscience. *J. Am. Chem. Soc.* **2010**, *132*, 5761−5768.
(35) Lesniak, A.; Fenaroli, F.; Monopoli, M. P.; Åberg, C.; Dawson, K. A.; Salvati, A. Effects of the Presence or Absence of a Protein Corona on Silica Nanoparticle Uptake and Impact on Cells. *ACS Nano* **2012**, *6*, 5845−5857.
(36) Schöttler, S.; Klein, K.; Landfester, K.; Mailänder, V. Protein Source and Choice of Anticoagulant Decisively Affect Nanoparticle Protein Corona and Cellular Uptake. *Nanoscale* **2016**, *8*, 5526−5536.
(37) Izak-Nau, E.; Voetz, M.; Eiden, S.; Duschl, A.; Puntes, V. F. Altered Characteristics of Silica Nanoparticles in Bovine and Human Serum: The Importance of Nanomaterial Characterization Prior to Its Toxicological Evaluation. *Part. Fibre Toxicol.* **2013**, *10*, 56−67.
(38) Piella, J.; Bastús, N. G.; Puntes, V. F. Size-Dependent Protein−Nanoparticle Interactions in Citrate-Stabilized Gold Nanoparticles: The Emergence of the Protein Corona. *Bioconjugate Chem.* **2017**, *28*, 88−97.
(39) Cho, E. C.; Zhang, Q.; Xia, Y. The Effect of Sedimentation and Diffusion on Cellular Uptake of Gold Nanoparticles. *Nat. Nanotechnol.* **2011**, *6*, 385−391.
(40) Panarella, A.; Bexiga, M. G.; Galea, G.; O'Neill, E. D.; Salvati, A.; Dawson, K. A.; Simpson, J. C. A Systematic High-Content Screening Microscopy Approach Reveals Key Roles for Rab33b, OATL1 and Myo6 in Nanoparticle Trafficking in HeLa Cells. *Sci. Rep.* **2016**, *6*, 28865.
(41) Rejman, J.; Oberle, V.; Zuhorn, I. S.; Hoekstra, D. Size-Dependent Internalization of Particles *via* the Pathways of Clathrin- and Caveolae-Mediated Endocytosis. *Biochem. J.* **2004**, *377*, 159−169.
(42) Al Soraj, M.; He, L.; Peynshaert, K.; Cousaert, J.; Vercauteren, D.; Braeckmans, K.; De Smedt, S. C.; Jones, A. T. SiRNA and Pharmacological Inhibition of Endocytic Pathways to Characterize the Differential Role of Macropinocytosis and the Actin Cytoskeleton on Cellular Uptake of Dextran and Cationic Cell Penetrating Peptides Octaarginine (R8) and HIV-Tat. *J. Controlled Release* **2012**, *161*, 132−141.
(43) Kim, J. A.; Åberg, C.; Salvati, A.; Dawson, K. A. Role of Cell Cycle on the Cellular Uptake and Dilution of Nanoparticles in a Cell Population. *Nat. Nanotechnol.* **2012**, *7*, 62−68.
(44) Shapero, K.; Fenaroli, F.; Lynch, I.; Cottell, D. C.; Salvati, A.; Dawson, K. A. Time and Space Resolved Uptake Study of Silica Nanoparticles by Human Cells. *Mol. BioSyst.* **2011**, *7*, 371−378.
(45) Agarwal, R.; Singh, V.; Jurney, P.; Shi, L.; Sreenivasan, S. V.; Roy, K. Mammalian Cells Preferentially Internalize Hydrogel Nanodiscs over Nanorods and Use Shape-Specific Uptake Mechanisms. *Proc. Natl. Acad. Sci. U. S. A.* **2013**, *110*, 17247−17252.
(46) Vercauteren, D.; Vandenbroucke, R. E.; Jones, A. T.; Rejman, J.; Demeester, J.; De Smedt, S. C.; Sanders, N. N.; Braeckmans, K. The Use of Inhibitors to Study Endocytic Pathways of Gene Carriers : Optimization and Pitfalls. *Mol. Ther.* **2010**, *18*, 561−569.
(47) dos Santos, T.; Varela, J.; Lynch, I.; Salvati, A.; Dawson, K. A. Quantitative Assessment of the Comparative Nanoparticle-Uptake Efficiency of a Range of Cell Lines. *Small* **2011**, *7*, 3341−3349.
(48) Dausend, J.; Musyanovych, A.; Dass, M.; Walther, P.; Schrezenmeier, H.; Landfester, K.; Mailänder, V. Uptake Mechanism of Oppositely Charged Fluorescent Nanoparticles in Hela Cells. *Macromol. Biosci.* **2008**, *8*, 1135−1143.
(49) Francia, V.; Reker-Smit, C.; Boel, G.; Salvati, A. Limits and Challenges in Using Transport Inhibitors to Characterize How Nano-Sized Drug Carriers Enter Cells. *Nanomedicine (London, U. K.)* **2019**, *14*, 1533−1549.
(50) Lesniak, A.; Salvati, A.; Santos-Martinez, M. J.; Radomski, M. W.; Dawson, K. A.; Åberg, C. Nanoparticle Adhesion to the Cell Membrane and Its Effect on Nanoparticle Uptake Efficiency. *J. Am. Chem. Soc.* **2013**, *135*, 1438−1444.
(51) Blanco, E.; Shen, H.; Ferrari, M. Principles of Nanoparticle Design for Overcoming Biological Barriers to Drug Delivery. *Nat. Biotechnol.* **2015**, *33*, 941−951.
(52) Goldstein, J. L.; Anderson, R. G.; Brown, M. S. Receptor-Mediated Endocytosis and the Cellular Uptake of Low Density Lipoprotein. *Ciba Found. Symp.* **2008**, *92*, 77−95.
(53) Koivusalo, M.; Welch, C.; Hayashi, H.; Scott, C. C.; Kim, M.; Alexander, T.; Touret, N.; Hahn, K. M.; Grinstein, S. Amiloride Inhibits Macropinocytosis by Lowering Submembranous pH and Preventing Rac1 and Cdc42 Signaling. *J. Cell Biol.* **2010**, *188*, 547−563.
(54) Lim, J. P.; Gleeson, P. A. Macropinocytosis: An Endocytic Pathway for Internalising Large Gulps. *Immunol. Cell Biol.* **2011**, *89*, 836−843.
(55) Lee, E.; Knecht, D. A. Visualization of Actin Dynamics During Macropinocytosis and Exocytosis. *Traffic* **2002**, *3*, 186−192.
(56) Bannunah, A. M.; Vllasaliu, D.; Lord, J.; Stolnik, S. Mechanisms of Nanoparticle Internalization and Transport Across an Intestinal Epithelial Cell Model: Effect of Size and Surface Charge. *Mol. Pharmaceutics* **2014**, *11*, 4363−4373.
(57) Marks, D. L.; Singh, R. D.; Choudhury, A.; Wheatley, C. L.; Pagano, R. E. Use of Fluorescent Sphingolipid Analogs to Study Lipid Transport along the Endocytic Pathway. *Methods* **2005**, *36*, 186−195.
(58) Kirchhausen, T.; Macia, E.; Pelish, H. E. Use of Dynasore, the Small Molecule Inhibitor of Dynamin, in the Regulation of Endocytosis. *Methods Enzymol.* **2008**, *438*, 77−93.
(59) Macia, E.; Ehrlich, M.; Massol, R.; Boucrot, E.; Brunner, C.; Kirchhausen, T. Dynasore, a Cell-Permeable Inhibitor of Dynamin. *Dev. Cell* **2006**, *10*, 839−850.
(60) Hoebeke, J.; Van Nijen, G.; De Brabander, M. Interaction of Oncodazole (R 17934), a New Anti-Tumoral Drug, with Rat Brain Tubulin. *Biochem. Biophys. Res. Commun.* **1976**, *69*, 319−324.
(61) Schliwa, M. Action of Cytochalasin D on Cytoskeletal Networks. *J. Cell Biol.* **1982**, *92*, 79−91.
(62) Boulant, S.; Kural, C.; Zeeh, J. C.; Ubelmann, F.; Kirchhausen, T. Actin Dynamics Counteract Membrane Tension During Clathrin-Mediated Endocytosis. *Nat. Cell Biol.* **2011**, *13*, 1124−1132.
(63) Sverdlov, M.; Shajahan, A. N.; Minshall, R. D. Tyrosine Phosphorylation-Dependence of Caveolae-Mediated Endocytosis: Caveolae Review Series. *J. Cell. Mol. Med.* **2007**, *11*, 1239−1250.
(64) Mazzolini, J.; Weber, R. J. M.; Chen, H. S.; Khan, A.; Guggenheim, E.; Shaw, R. K.; Chipman, J. K.; Viant, M. R.; Rappoport, J. Z. Protein Corona Modulates Uptake and Toxicity of

DOI: 10.1021/acsnano.9b03824
ACS Nano 2019, 13, 11107−11121

Nanoceria *via* Clathrin-Mediated Endocytosis. *Biol. Bull.* **2016**, *231*, 40−60.
(65) Digiacomo, L.; Cardarelli, F.; Pozzi, D.; Palchetti, S.; Digman, M. A.; Gratton, E.; Capriotti, A. L.; Mahmoudi, M.; Caracciolo, G. Apolipoprotein-Enriched Biomolecular Corona Switches the Cellular Uptake Mechanism and Trafficking Pathway of Lipid Nanoparticles. *Nanoscale* **2017**, *9*, 17254−17262.
(66) Walkey, C. D.; Chan, W. C. W. Understanding and Controlling the Interaction of Nanomaterials with Proteins in a Physiological Environment. *Chem. Soc. Rev.* **2012**, *41*, 2780−2799.
(67) Kim, J. A.; Salvati, A.; Åberg, C.; Dawson, K. A. Suppression of Nanoparticle Cytotoxicity Approaching *In Vivo* Serum Concentrations: Limitations of *In Vitro* Testing for Nanosafety. *Nanoscale* **2014**, *6*, 14180−14184.
(68) Fedeli, C.; Segat, D.; Tavano, R.; Bubacco, L.; De Franceschi, G.; de Laureto, P. P.; Lubian, E.; Selvestrel, F.; Mancin, F.; Papini, E. The Functional Dissection of the Plasma Corona of SiO_2-NPs Spots Histidine Rich Glycoprotein As a Major Player Able to Hamper Nanoparticle Capture by Macrophages. *Nanoscale* **2015**, *7*, 17710−17728.
(69) Kelly, P. M.; Åberg, C.; Polo, E.; O'Connell, A.; Cookman, J.; Fallon, J.; Krpetić, Ž.; Dawson, K. A. Mapping Protein Binding Sites on the Biomolecular Corona of Nanoparticles. *Nat. Nanotechnol.* **2015**, *10*, 472−479.
(70) Stewart, J. C. M. Colorimetric Determination of Phospholipids with Ammonium Ferrothiocyanate. *Anal. Biochem.* **1980**, *104*, 10−14.

DOI: 10.1021/acsnano.9b03824
ACS Nano 2019, 13, 11107−11121